20.7 An SpO_2 Sensor Using Reconstruction-Free Sparse Sampling for 70% System Power Reduction

Sina Faraji Alamouti[1], Cem Yalcin[1], Jasmine Jan[1], Jonathan Ting[1], Ana C. Arias[1], Rikky Muller[1,2]

[1]University of California, Berkeley, CA
[2]Chan Zuckerberg Biohub, San Francisco, CA

Low arterial blood oxygenation (SpO_2) is a measure of hypoxemia and a sign of problems relating to breathing and circulation. Progressive drop in arterial SpO_2 can be an early indicator of severe disease in COVID-19 patients [1]. A hypoxic state can occur rapidly and without a patient's knowledge; therefore, early detection of SpO_2 decline can be lifesaving. In other respiratory system diseases such as COPD and sleep apnea, continuously monitoring of SpO_2 with a pulse oximeter can enable timely diagnosis of oxygen desaturation. SpO_2 is measured with Photoplethysmography (PPG) that uses a photodetector (PD) to detect either the transmission or reflection of light from the surface of the skin at two different light wavelengths. Commercial fingertip SpO_2 sensors are not designed for chronic wear and require user intervention to trigger measurements. Alternatively, wearable SpO_2 recording devices in the form of watches and rings can operate in the background with minimal user intervention. However, continuous acquisition of SpO_2 can present a significant power burden to a wearable device since high-power LEDs must be powered on for each sample, dominating the power dissipation of the sensor. We present a low-power pulse oximeter sensor IC that utilizes sparse sampling to reduce the overall power by 70%.

Figure 20.7.1 shows the system and the IC block diagram. To perform reflectance mode oximetry, two LEDs at red (R – 660nm) and infrared (IR – 880nm) wavelengths, and a PD are placed on the same side above the tissue. The LEDs are powered on sequentially by on-chip drivers. Their reflected light is captured by the PDs, and a mixed-signal transimpedance front-end (TFE) acquires the photogenerated PD current on up to 8 channels, while an on-chip digital backend (DBE) performs signal calculations, controls the DAC in closed-loop and provides timing.

Traditional SpO_2 sensors consume mWs of power to drive the LEDs, limiting the battery life. To reduce LED power, prior art has utilized low duty cycles [2-5]. For <2% SpO_2 error, SNR >39dB is required [9], limiting the lower bound on LED duty cycle. Sparse sampling was previously proposed to reduce the effective PPG sample rate, and therefore LED power for heart rate (HR) and variability (HRV) measurements [6]. However, extending that technique to the extraction of SpO_2 from randomly compressed samples requires full signal reconstruction that can dissipate up to 10mW [6]. Heartbeat locking was also introduced in [7] to track HR and HRV with extremely low LED power consumptions, but since the PPG data was not sampled, no SpO_2 measurements could be provided. In this work, LED power is reduced by implementing a reconstruction-free sparse sampling technique to reduce the LED power consumption by 75%, and the total system power consumption by 70% while maintaining <1% SpO_2 error.

Figure 20.7.2 shows the detailed IC block diagram for the sensor. At the input, an 8b differential current DAC (5b thermometer, 3b binary-coded) subtracts the DC component of the signal up to 15μA, relaxing the front-end dynamic range requirements, while digitizing the DC value. The fully differential readout eliminates any PD voltage bias induced noise components and improves common-mode effects rejection. The AC current is then amplified via a TIA. To accommodate a wide range of PD configurations and overcome the impact of PD parasitic capacitance (C_{par}=40pF to 10nF) on the noise transfer function, a ZTIA topology that has both resistive and capacitive feedback branches is used as CTIA topologies suffer from increased noise penalties in presence of large input parasitics [5]. A high-gain, three-stage, current-reuse core OTA is designed to suppress the input-referred noise (IRN) and improve settling speed. The feedback resistor in this topology enhances the feedback factor at lower frequencies, thereby lowering the noise at the TIA output. Flicker noise is minimized by upsizing the input devices and system level correlated double sampling. A reset integrator provides adjustable gain and boxcar averaging, removing the increased high frequency noise of the TIA and mitigates the need for explicit anti-alias filtering. Combined with ZTIA gain, an overall adjustable forward path gain of 1 to 40M is achieved. The resulting voltage is then sampled and digitized by a 12b synchronous SAR ADC. In the backend, the digitized AC signal is accumulated to form the DC-cancellation DAC codes, closing the servo loop and providing high-pass filtering. To alleviate P- and N-DAC mismatch, the feedback gain coefficients are separately calibrated. The timing diagram of the sensor is also shown in Fig. 20.7.2. Each phase starts with a short reset period to initialize the TFE subblocks. Ambient light is also separately sampled, digitized, and subtracted from the signal values to improve accuracy.

SpO_2 (Fig. 20.7.3, Eq. 1) is computed based on the ratio of pulsatile (AC) over the baseline (DC) component of the PPG waveform for the R and IR wavelengths. The computation requires only the PPG peaks and valleys (PAV), therefore in principle few samples, centered around the PAVs, are required. We implement an on-chip algorithm that reduces the total samples to only capture PAVs. Figure 20.7.3 describes the implemented algorithm. In Phase 1, uniform sampling is performed at 100Hz and the PPG signal period (T) is learned. The sensor then transitions to sparse mode (Phase 2) and samples only around predicted PAV locations. Initially, a window size (W) of [T/8] samples per PAV is selected. Successful detection of PAVs allows the DBE to reduce W to save power and update the estimated T. Using this technique, the total number of samples required for SpO_2 and HR extraction is decreased by ~4×, resulting in ~70% overall power reduction.

Large motion artifacts can cause repeated missed detections of PAVs. When this occurs, the DBE will increase W to expand the observation window until new PAVs are found. If new PAVs are not found after W reaches W_{max} (programmable), the system will revert to Phase 1 for re-estimation of the PPG period as shown in the Fig. 20.7.3 flowgraph.

The IC was taped out in TSMC's 40nm HV process and the chip microphotograph is shown in Fig. 20.7.7. The chip occupies 1.35×1.8mm^2 and consists of two readout channels. In continuous mode, TFE, DBE, and LEDs consume 1.22μW, 3.34μW, and 45.1μW respectively. Sparse mode lowers the power consumption of TFE and LEDs to 0.32μW and 11.4μW while increasing the DBE power by only ~2% to 3.43μW.

Figure 20.7.4 shows the measured input-referred noise (IRN) spectral density of the TFE for C_{par}=40 pF (matching the C_{pd} used in this system), which is 4.8pA$_{rms}$/√Hz when the sensor is operating in continuous mode. The minimum PPG AC amplitude at the input is approximately 4nA$_{pp}$, which results in a SNR of 41dB. This amplitude can increase with an increased LED drive current. IRN increases as C_{par} increases, and the LED drive current can scale with C_{par} to maintain SNR. Figure 20.7.4 also shows the spectrum of the ADC output for a 2Hz sine wave input current and C_{par}=40pF. An SNDR of 62.41dB and an SFDR of 68.33dB are achieved with a 50nA$_{pp}$ input. In sparse mode, SpO_2 and HR accuracy are reported instead of noise and linearity since no reconstruction is done. A set of *in vivo* experimental results are shown in Fig. 20.7.5 with the sensor placed on the index finger of a healthy user in a sitting position under typical incandescent lighting, and at room temperature and compared to a clinical grade sensor (Wellue HPO) placed on the ring finger. This work achieves <1% error of SpO_2 and <1bpm error in HR measurements when compared with the clinical sensor in both continuous and sparse modes. The mean absolute errors in each mode are listed in the table in Fig. 20.7.6.

We introduce a reconstruction-free, sparse sampling technique to record SpO_2 and HR at 70% overall power reduction with <1% loss in accuracy. Figure 20.7.6 shows a comparison with recent PPG/HR/SpO_2 sensor interfaces, including heart-beat locked [7] and compressively sampled [8] sensors. When used in sparse mode, this work simultaneously achieves the lowest input-referred noise, the lowest HR and SpO_2 error rates, and the lowest total system power consumption by 2.7×, compared to entries in the table.

Acknowledgment:
The authors thank NextFlex institute, the sponsors of BWRC and TSMC for chip fabrication. Thanks to M. Meraj Ghanbari for technical discussion.

References:
[1] R.G. Wilkerson, et al., "Silent Hypoxia: A Harbinger of Clinical Deterioration in Patients with COVID-19," *Am. J. Emerg. Med.*, vol. 38, no. 10, pp. 2243.e5-2243.e6, Oct. 2020.
[2] M. Konijnenburg, et al., "A 769μW Battery-Powered Single-Chip SoC With BLE for Multi-Modal Vital Sign Health Patches," *ISSCC Dig. Tech. Papers*, pp. 360-361, Feb. 2019.
[3] A. Caizzone, et al., "A 2.6 μW Monolithic CMOS Photoplethysmographic (PPG) Sensor Operating With 2 μW LED Power for Continuous Health Monitoring," *IEEE TBioCAS*, vol. 13, no. 6, pp. 1243-1253, 2019.
[4] F. Marefat, et al., "A 280μW 108dB DR Readout IC with Wireless Capacitive Powering Using a Dual-Output Regulating Rectifier for Implantable PPG Recording," *ISSCC Dig. Tech. Papers*, pp. 412-413, Feb. 2020.
[5] Y. Lee, et al., "A 141μW Sensor SoC on OLED/OPD Substrate for SpO2/ExG Monitoring Sticker," *ISSCC Dig. Tech. Papers*, pp. 384-385, Feb. 2016.
[6] V.R. Pamula, et al., "A 172μW Compressively Sampled Photoplethysmographic (PPG) Readout ASIC With Heart Rate Estimation Directly from Compressively Sampled Data," *IEEE TBioCAS*, vol. 11, no. 3, pp. 487-496, 2017.
[7] D.-H. Jang and S.H. Cho, "A 43.4μW Photoplethysmogram-Based Heart-Rate Sensor Using Heart-Beat-Locked Loop," *ISSCC Dig. Tech. Papers*, pp. 474-475, Feb. 2018.
[8] S.-J. Jung, et al., "A 400-to-1000nm 24μW Monolithic PPG Sensor with 0.3A/W Spectral Responsivity for Miniature Wearables," *ISSCC Dig. Tech. Papers*, pp. 388-389, Feb. 2021.
[9] K.N. Glaros, et al., "A sub-mW Fully-Integrated Pulse Oximeter Front-End," *IEEE TBioCAS*, vol. 7, no. 3, pp. 363-375, 2012.

2022 IEEE International Solid- State Circuits Conference (ISSCC) | 978-1-6654-2800-2/22/$31.00 ©2022 IEEE | DOI: 10.1109/ISSCC42614.2022.9731113

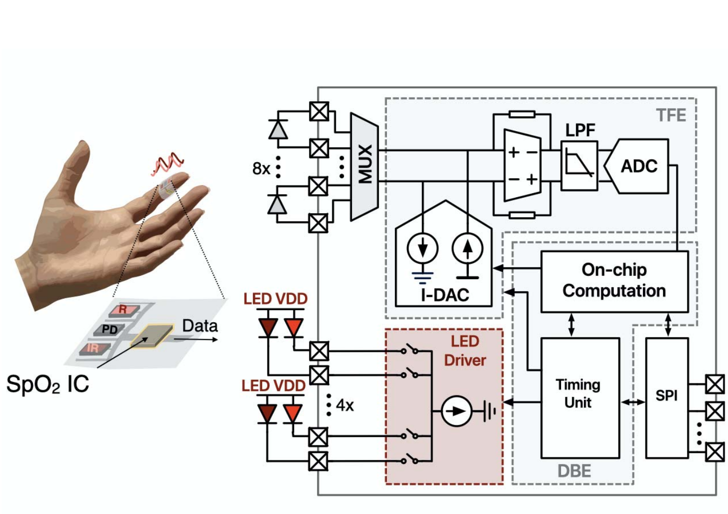

Figure 20.7.1: An SpO$_2$ monitoring sensor is shown that consists of an SpO$_2$ readout IC and sensor devices.

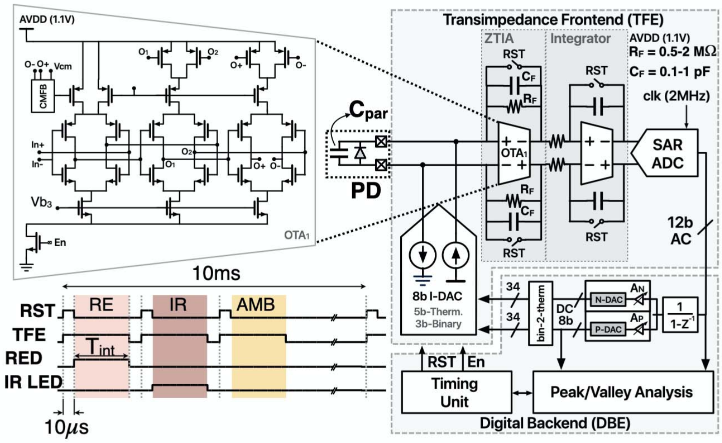

Figure 20.7.2: Detailed block diagram of the TFE as well as the timing diagram. The left insets show the schematic of the three-stage current reuse OTA. The DBE controls the timing, computes the DAC codes and evaluates the received samples for sparse-mode sampling.

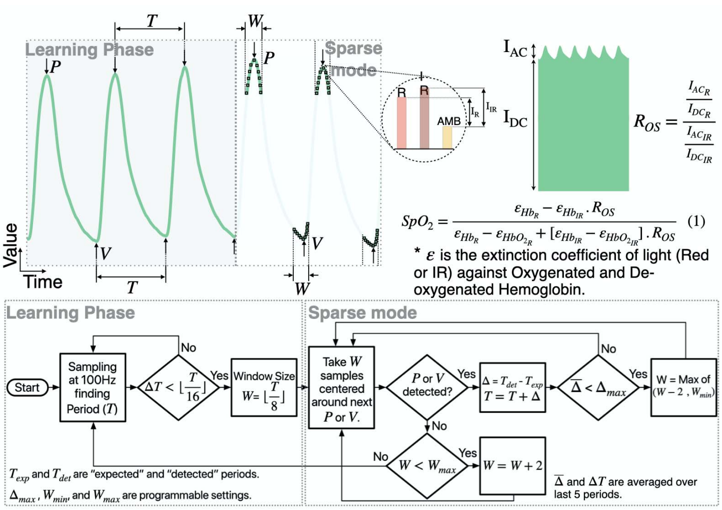

Figure 20.7.3: Details of the sparse sampling technique. (Top) Learning of period and transition to sparse mode and the computations for SpO$_2$. (Bottom) Flowchart of the sparse algorithm to capture PAV.

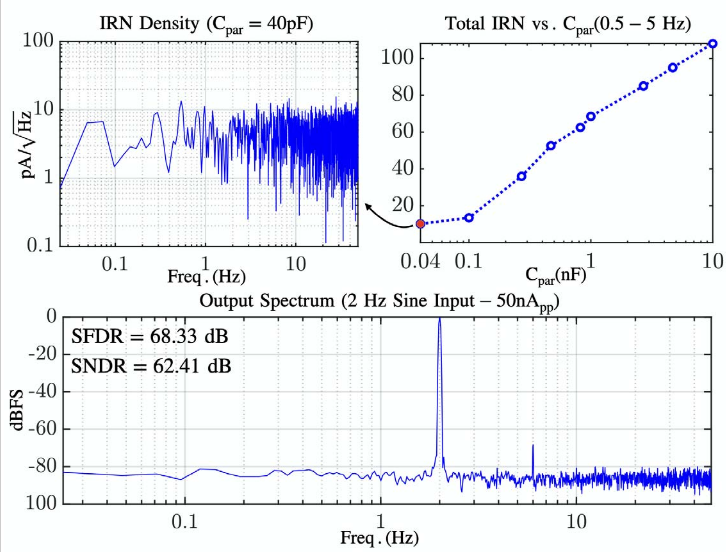

Figure 20.7.4: Electrical testing results. (Top) Input-referred noise spectrum for C_{par} = 40pF as well as the total integrated current noise versus C_{par}. (Bottom) ADC output spectrum plot with a 2Hz, 50nA$_{pp}$ sine wave input.

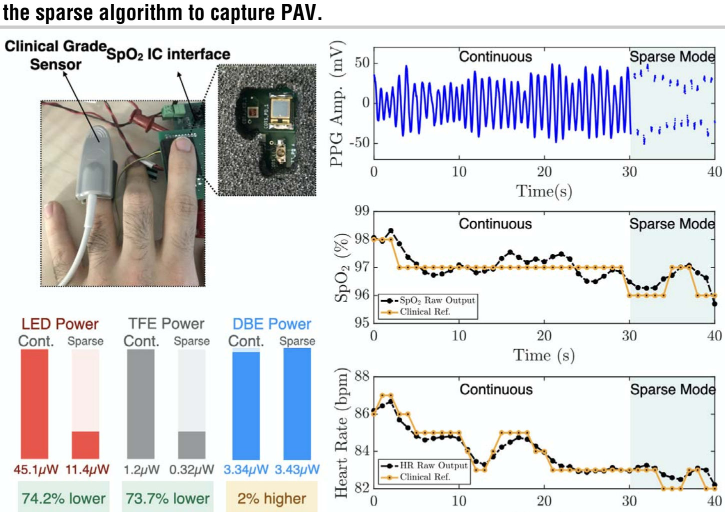

Figure 20.7.5: *In vivo* measurement results. PPG waveform, SpO$_2$ and HR results from a sample recording with both continuous and sparse modes are shown and compared against reference values (Right). Setup is shown with both SpO$_2$ IC and clinical-grade sensor (Top Left). Power break-down is shown for continuous and sparse modes (Bottom left).

	ISSCC 2016 [5]	TBioCAS 2017 [6]	ISSCC 2018 [7]	ISSCC 2019 [2]	TBioCAS 2019 [3]	ISSCC 2020 [4]	ISSCC 2021 [8]	This Work	
								Continuous Mode	Sparse Mode
Technology (nm)	180	180	180	55	180	180	65	40 HV	
VDD (LED/Readout)	5/1.5	5/1.2	3.3	2.8/1.2	3.3/1.8	2.5/1.5	1.8/1	5/1.1	
Readout Power (µW/Ch)	87[a]	172	27.4	54	2.63	15.7	24	TFE: 1.22 DBE: 3.34	TFE: 0.32 DBE: 3.43
LED Power (µW)	54[a,d]	120[c]	16	827	44	264	18[a]	45.1	11.4
Total Power (µW)	141	292	43.4	881	46.63	279	42[a]	49.66	15.15
Sampling freq. (Hz)	400	128	100	128	40	250	20	100	
Duty Cycle (%)	2	0.4	0.25	-	0.07	3.2	0.04	0.25	
Input noise (pA/rtHz)	-	153	-	6.3	-	73[a]	-	4.8[e]	
SpO2 Error (%)	2[b]	-	-	-	-	-	-	0.5[f]	0.7[f]
HR Error (bpm)	-	2[b]	2.1[f]	-	1.4[f]	-	1.9[f]	0.3[f]	0.4[f]

[a] Estimated values. [b] Maximum error. [c] For 10x Compression Rate. [d] With Organic LEDs/PDs [e] Cpar = 40pF (matching Cpd) [f] Mean Abs. error

Figure 20.7.6: Table of comparison including recent PPG/SpO$_2$/HR sensors.

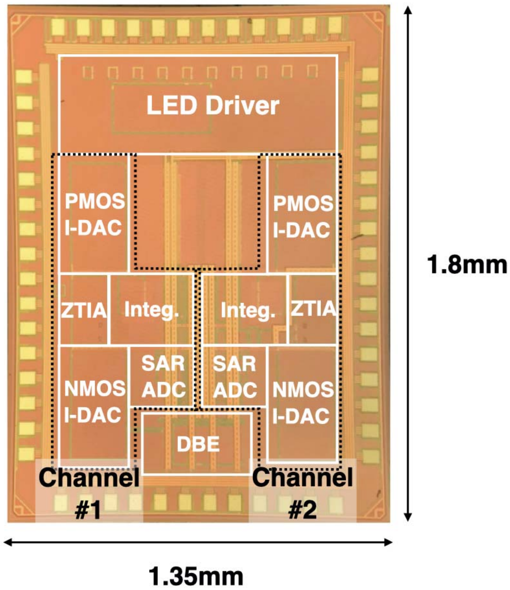

Figure 20.7.7: Chip micrograph.

978-1-6654-2800-2/22/$31.00 ©2022 IEEE